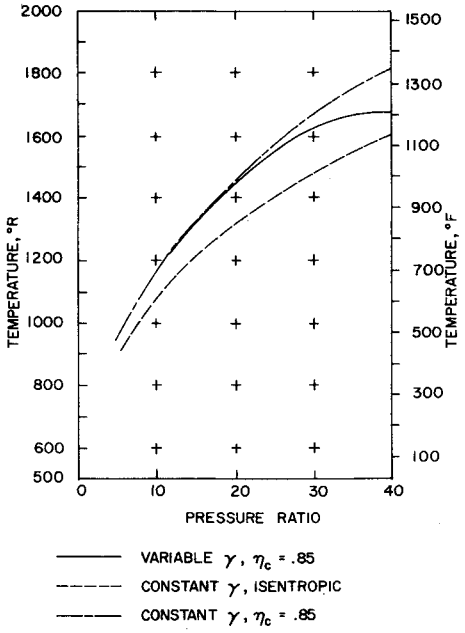

Fig. 2 Compressor exit temperature vs pressure ratio; inlet T_T = 300°K.

θ_V is 2230°K. A graph of Eq. (1) is given in Fig. 1. It is apparent that when $\theta_V/2T = 3$, the vibration is about 10% excited. This occurs at 372°K or about 250°F. At 1660°F vibrational degrees of freedom in oxygen are 72% excited.

Compressor efficiency η_c is usually defined as

$$\eta_c = [\pi_c^{(\gamma-1)/\gamma} - 1]/(\tau_c - 1) \quad (2)$$

where π_c is stagnation pressure ratio and τ_c, the stagnation temperature ratio of the compressor. When real gas effects occur, a reasonable extension of the definition is

$$\eta_c = [\pi_c^{(\gamma-1)/\gamma} - 1]/(h_c - 1) \quad (3)$$

where γ is evaluated at the compressor inlet conditions and the symbol h_c represents the ratio of stagnation enthalpies.

Figure 2 is a plot of compressor exit temperature as a function of pressure ratio. Inlet stagnation temperature was taken as 300°K. The Mollier diagram for air from Little's report[1] was used to find exit values with variable γ. Notice that for pressure ratios to 30, the influence of variable γ is very slight. However, at 40, an error in temperature of about 10% results assuming constant γ.

It has long been recognized that variable γ is essential for describing processes in the hot section of the engine. For low pressure ratio engines, an assumption of constant γ for the compressor has been adequate. As seen in Fig. 2, for $\pi_c > 30$, proper analysis requires a variable γ.

In order to point out the significance of Fig. 2, a few aspects of compressor technology will be considered. Some instruments measure temperature; others measure enthalpy. Precision compressor testing at high π_c requires careful selection of instrumentation. Furthermore, interpretation of performance data should include enthalpy. Compressor efficiency based on τ_c is obviously more favorable than η_c based on h_c. Equation (3) yields a valid representation of over-all compressor losses. The compressor discharge air is used to cool the turbine blades. Cooling analysis and testing need to be based on compressor discharge enthalpy rather than temperature when $\pi_c > 30$. Current practice is to report cooling data in terms of temperature.[2] Transport properties, e.g., thermal conductivity, and dimensionless groups formed from transport properties, e.g., Prandtl number, change significantly when internal degrees of freedom are excited.[3] A new approach for making point temperature measurements with fast time response is to use Raman scattering. Widhoff and Lederman[4] have demonstrated use of Raman scattering to measure species concentration. An extension of this approach will yield temperature. Above π_c of 30, the experimentalist has the choice of using Stokes or anti-Stokes vibrational bands to ascertain temperature. Finally, if one wants to understand combustion kinetics from a fundamental point of view, the presence of vibrationally excited O_2 in the combustor inlet is important. High pressure ratios are here today, e.g., JT9D has π_c = 24.5. The trend is to higher values. Real gas effects will become a factor to consider.

References

[1] Little, W. J., "Mollier Chart for Air," AEDC-TDR-63-190, Sept. 1963, von Kármán Gas Dynamics Facility, Arnold Engineering Development Center.

[2] "AGARD Conference Proceedings," *High Temperature Turbines*, No. 73, Sept. 1970.

[3] Hirschfelder, J. O., Curtiss, C. F., and Bird, R. B., *Molecular Theory of Gases and Liquids*, Wiley, New York, 1954.

[4] Widhoff, G. F. and Lederman, S., "Specie Concentration Measurements Utilizing Raman Scattering of a Laser Beam," *AIAA Journal*, Vol. 9, No. 2, Feb. 1971, pp. 309–316.

Pulsed Air Gust Generator

JOSEPH BICKNELL*
Texas A&M University, College Station, Texas

Nomenclature

a	=	speed of sound
A_j	=	discharge area of all jet nozzles
A_t	=	tunnel test section area
K	=	$\omega/a\beta^2$
$\dot{m}$	=	mass flow rate of all nozzles
$\dot{m}_0$	=	twice the time average $\dot{m}$
M	=	Mach number
p	=	ambient absolute pressure
Δp	=	pressure perturbation
R	=	$[(x-\xi)^2 + (y-\eta)^2 + (z-\xi)^2]^{1/2}$
t	=	time
U	=	average axial velocity
ΔU	=	axial perturbation
V_j	=	discharge velocity of jet nozzle
x,y,z	=	coordinates of point in tunnel
β	=	$(1 - M^2)^{1/2}$
γ	=	ratio of specific heats
ρ	=	mass density
ϕ	=	velocity potential
ω	=	circular frequency, rad/sec
ξ,η,ζ	=	coordinates of point source

VARIOUS methods have been developed and used to produce oscillating airflows as tools for research on unsteady aerodynamics. Examples are oscillating wall mounted airfoils to produce lateral disturbances, and rotating shutters to produce longitudinal waves.[1] Thomas[2] carried out pilot testing on an array of jets downstream of the test section arranged to blow cyclically with time either upstream or downstream. This report concerns the calibration tests of an improved apparatus installed in a larger wind tunnel.

Presented as Paper 71-281 at the AIAA 6th Aerodynamic Testing Conference, Albuquerque, New Mexico, March 10–12, 1971; submitted April 1, 1971; revision received June 1, 1971. Early development of the pulsed air gust generator was sponsored by NASA, Langley Research Center. Later work was supported by the U.S. Army Research Office, Durham, under Themis Contract DAHCO4-69-0015.

Index Category: Nonsteady Aerodynamics.

* Visiting Professor, Aerospace Engineering Department. Member AIAA.

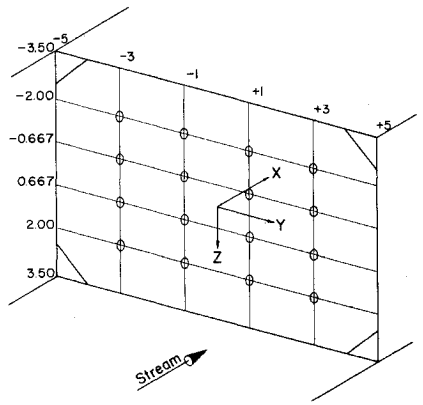

Fig. 1 Nozzle array and axis system.

An analytical model of the wave producing action was developed to gain insight into the process and what might be expected of it. The jet action was modelled by two effects: the volume effect by a distribution of time dependent sources, the momentum flux by an equivalent plane pressure source acting in the streamwise direction. The latter action can be described as follows. The upstream momentum flux is conveyed through mixing into the oncoming stream, producing an equivalent plane pressure source in phase with and having the amplitude of the momentum discharged/unit cross-section area of the tunnel at the mixing region. These pressure waves then propagate throughout the tunnel at sound velocity. It is apparent that the resultant response of the tunnel flow is difficult if not impossible to compute, but one would expect the response to be frequency dependent. A compression wave travelling upstream is accompanied by an expansion wave travelling downstream, to meet in the return section of the tunnel and again in the test section. These disturbances differ from atmospheric gustiness in that they have their own propagation velocity with respect to the convecting stream.

The source effect can be represented by an array of sinusoidally varying point sources in a constant cross section infinitely long duct and sets of this array outside of the duct to represent the effect of the duct walls. The potential at x,y,z of a point source at ξ,η,ζ is[3] ϕ, where

$$4\pi\phi = -R^{-1}\exp[ikM(x-\xi) - ikR + i\omega t]$$

The $+X$ axis is downstream, the $+Y$ axis horizontal and the $+Z$ axis downward (see Fig. 1). The symbol R denotes the distance between x,y,z and ξ,η,ζ.

The sources produce waves travelling at sound velocity $\pm$ tunnel velocity depending on whether downstream or upstream waves are considered. The results of computations for unit volume amplitude sources showed that the non-uniformity of the disturbance velocity magnitude along the duct centerline is less than 4%. Off centerline positions of

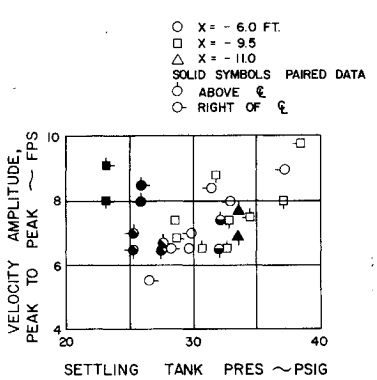

Fig. 2 Amplitude response (39HZ).

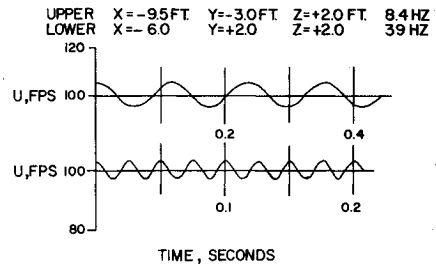

Fig. 3 Disturbance wave forms.

$Y = 2$ and 4 ft for $Z = 0$ and for $Y = Z = 2$ ft at $X = -8$ ft showed variations in the velocity of less than 1.0% from the centerline value.

For the momentum effects assume that all the momentum flux is simultaneously converted through turbulent mixing to a pressure in the stream direction, so that $\dot{m}V_j = A_t\Delta p$. For a plane pressure wave, the particle velocity is related to the pressure disturbance by $\Delta p/p = -\gamma\Delta U/a = \dot{m}V_j/pA_t$.

If the mass flow rate is in the form of a displaced cosine, the momentum efflux rate will be in the form of a squared displaced cosine and not sinusoidal. The disturbance velocity will likewise not be sinusoidal. The first valve design produced such wave forms. After considerable redesign and trial, the open period of the valve was increased and a more sinusoidal $\dot{m}V_j$ was produced. The latter produces a non-sinusoidal source effect so some compromise, arrived at experimentally, was effected.

For a representative operating condition, nozzle upstream pressure 30 psig, peak mass flow rate 46.7 lb/sec (all nozzles), estimated peak momentum flux of 955 lb. Peak to peak velocity disturbance due to momentum were 5.12 fps and from source effect 3.23 fps, giving a total (assuming the same phase relation) of 8.35 fps. Measured values are about 8 fps. One should realize the large pressure amplitude associated with this disturbance is about 13 psf.

The apparatus was installed in the Texas A&M University's 7-ft × 10-ft wind tunnel, a closed return tunnel with a contraction ratio of 10 and the rather long centerline length of 420 ft. The jet array is made up of 16 nozzles, 4 on each of 4 supply pipes installed across the test section near the downstream end. Rotary plug valves near the nozzles are used to modulate the jet flow. The valves are driven by a variable speed motor and are capable of pulsing frequencies up to 65 Hz.

Storage tanks and a manually operated throttling valve supply air to stilling tanks on both sides of the test section.

Tests were run by setting the tunnel velocity at 125 fps then starting the pulsating nozzle flow. The mean airspeed dropped to about 100 fps with no attempt made to regulate it. Previous tests showed that the wave amplitudes were independent of mean tunnel velocity in agreement with the analytical model. As the tunnel speed decreases, the jet mixing region length increases, however.

Calibration tests were run at frequencies at which the tunnel responded favorably, a typical low value of 8 Hz and a high value of 39 Hz. Reference tank pressure, phase of valves and longitudinal velocity were recorded for a representative region of the test section. The velocity amplitude vs tank pressure is shown in Fig. 2. The scatter is attributed to the lack of equilibrium due to the long response time of the tunnel. When simultaneous data at two points were taken (paired data), the disparity between the points was small, 0.5 fps or less. This uniformity applies to a central region of about 60% of the tunnel width and height and for an axial distance of about 5 ft. Moving the generator into the diffuser would permit larger axial test regions. Only a slow deterioration of the disturbance uniformity occurred as the walls were approached.

Peak to peak amplitudes of 10 fps were obtained without structural reinforcement. Phase measurements showed that plane waves were moving upstream at near sound velocities. Wave forms were closely sinusoidal (see Fig. 3).

References

[1] Miller, J. A. and Fejer, A. A., "Transition Phenomena in Oscillating Boundary Layer Flows," *Journal of Fluid Mechanics*, Vol. 18, 1964, p. 438.

[2] Thomas, R. E. and Morland, B. T., Jr., "Gust Simulation in a Wind Tunnel," Space Technology Rept. 67-52, July 1967, Texas A&M Univ., College Station, Texas.

[3] Donovan, A. F. and Lawrence, H. R., ed., "Aerodynamic Components of Aircraft at High Speeds," *High Speed Aerodynamics and Jet Propulsion*, Vol. VII, Sec. F, Princeton University Press, 1957, pp. 671–675.

A Direct Matrix Method for the Divergence Problem

V. T. NAGARAJ*
Hindustan Aeronautics Ltd., Bangalore, India

Nomenclature

a = flexibility matrix
A = see Eq. (9)
B = see Eq. (9)
c = wing chord
C_h = aerodynamic influence coefficient matrix
$C_{L\alpha}$ = lift curve slope
$C_{m\alpha}$ = moment curve slope
C^z = translation flexibility (two-dimensional model)
C^α = rotational flexibility (two-dimensional model)
d = see Fig. 2
e = see Fig. 2
F = column matrix of control point forces
h = column matrix of the control point deflections
I = unit matrix
S = area of two-dimensional wing model
q = dynamic pressure

Introduction

IN the estimation of the divergence speed of a lifting surface, the usual procedure is to compute the moment, about a convenient reference axis, due to the aerodynamic forces and to equate this to the structural restoring moment. When the surface has a well defined elastic axis, this procedure is simple to apply and there are a number of methods for obtaining the divergence speed, if the bending and the torsional stiffnesses are known.[1] However, in many cases it may not be possible to separate the two effects and the stiffnesses are usually available in the form of a matrix of structural influence coefficients measured at a set of points on the surface. In the following, a method is given by which a direct solution can be obtained for the divergence speed using the matrices of the structural and the static aerodynamic influence coefficients.

Table 1 Symmetrical divergence of the wing of Fig. 3

Method	Divergence speed (fps)	Comments
Ref. 1	1948.2	Strip theory
Ref. 1	1823.1	Lifting line theory
Present	1583.2	One station at 268 in.
Present	1704.8	Two stations (186 in. and 368 in.)
Present	1919.2	Three stations (90 in., 268 in. and 468 in.)
Present	1925.1	Five stations (Fig. 3)
Present	1786.5	Five stations; lifting line theory

Received June 2, 1971.
* Project Engineer (Aeroelasticity). Member AIAA.

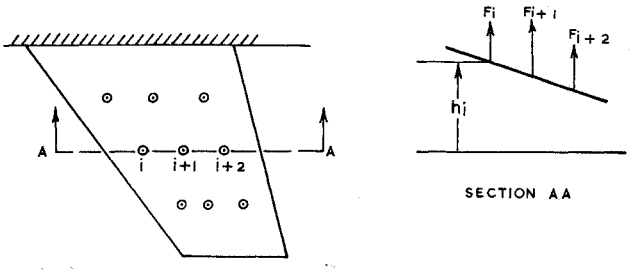

Fig. 1 Wing of general planform.

Outline of the Method

Consider the wing shown in Fig. 1. The control point deflections $\{h\}$ are related to the corresponding forces $\{F\}$ through the flexibility matrix as

$$\{h\} = [a]\{F\} \tag{1}$$

Let the matrix of static aerodynamic influence coefficients $[C_h]$ be defined by

$$\{F\}_{\text{aero}} = q[C_h]\{h\} \tag{2}$$

where $\{F\}_{\text{aero}}$ represents the column matrix of the aerodynamic forces at the control points. (A number of methods are available for computing the $[C_h]$ matrix for wings of arbitrary planform from subsonic to supersonic speeds.)

The value of the dynamic pressure at divergence is obtained when $\{F\}_{\text{aero}}$ in Eq. (2) is the same as the $\{F\}$ in Eq. (1). That is, when

$$[a]^{-1}\{h\} = q_D[C_h]\{h\} \tag{3}$$

or, in the standard form,

$$(1/q_D)\{h\} = [a][C_h]\{h\} \tag{4}$$

Equation (4) can be solved to obtain the divergence speed. The preceding method is illustrated by application to two subsonic torsional divergence problems in the following section.

Applications

1) The system to be analyzed is shown in Fig. 2a and consists of an aerofoil, restrained at a distance e behind the aerodynamic center by a translational spring of flexibility C^z and a torsional spring of flexibility C^α. For the present analysis, this system is replaced by the equivalent system shown in Fig. 2b. The forward and rear control points are located (arbitrarily) at the aerodynamic centre and at a distance d behind the elastic axis, respectively. For this system, the flexibility matrix is given by

$$[a] = \begin{bmatrix} C^z + e^2C^\alpha & C^z - ed & C^\alpha \\ C^z - edC^\alpha & C^z + d^2 & C^\alpha \end{bmatrix} \tag{5}$$

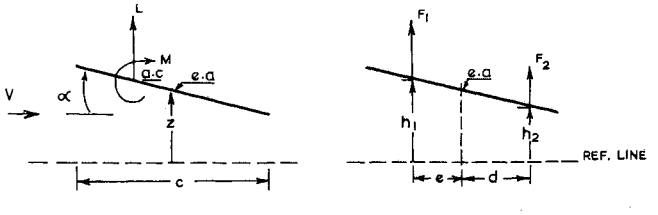

Fig. 2 Two-dimensional model wing.